Poly(*N*-isopropylacrylamide)-gated Fe$_3$O$_4$/SiO$_2$ core shell nanoparticles with expanded mesoporous structures for the temperature triggered release of lysozyme

Erick Yu [a,c], Irene Galiana [a], Ramón Martínez-Máñez [a,b,*], Pieter Stroeve [c,*], María D. Marcos [a,b], Elena Aznar [b], Félix Sancenón [a,b], José R. Murguía [a], Pedro Amorós [d]

[a] *Centro de Reconocimiento Molecular y Desarrollo Tecnológico (IDM), Unidad Mixta Universidad Politécnica de Valencia, Universidad de Valencia, Departamento de Química, Universidad Politécnica de Valencia, 46022 Valencia, Spain*
[b] *CIBER de Bioingeniería, Biomateriales y Nanomedicina (CIBER-BBN)*
[c] *Department of Chemical Engineering and Materials Science, University of California Davis, 95616 Davis, California, United States*
[d] *Institut de Ciència dels Materials (ICMUV), Universitat de València, P.P Box 2085, 46071 Valencia, Spain*

ARTICLE INFO

ABSTRACT

Core-shell nanoparticles comprised of Fe$_3$O$_4$ cores and a mesoporous silica shell with an average expanded pore size of 6.07 nm and coated with a poly(*N*-isopropylacrylamide) (PNIPAM) layer (CS–MSNs–EP–PNIPAM) were prepared and characterized. The nanoparticles was loaded with (Ru(bipy)$_3$$^{2+}$) dye or an antibacterial enzyme, lysozyme, to obtain CS–MSNs–EP–PNIPAM–Ru(bipy)$_3$$^{2+}$ and CS–MSNs–EP–PNIPAM–Lys, respectively. The lysozyme loading was determined to be 160 mg/g of nanoparticle. It was seen that Ru(bipy)$_3$$^{2+}$ and lysozyme release was minimal at a room temperature of 25 °C while at physiological temperature (37 °C), abrupt release was observed. The applicability of the CS–MSNs–EP–PNIPAM–Lys was further tested with two Gram-positive bacteria samples, *Bacillus cereus* and *Micrococcus luteus*. At physiological temperature, the nanoparticles were shown to reduce bacterial growth, indicating a successful release of lysozyme from the nanoparticles. This nanoparticle system shows potential as a nanocarrier for the loading of similarly sized proteins or other species as a drug delivery platform.

© 2015 Elsevier B.V. All rights reserved.

1. Introduction

New drug delivery systems capable of releasing active molecules in a controlled fashion have received significant attention recently [1–3]. In particular, among the potential delivery platform materials, such as polymers [4,5], liposomes [6,7], etc., mesoporous silica nanoparticles (MSNs) have been widely used as carriers for the storage and delivery of cargo species due to their distinctive properties, such as facile functionalization, high loading capacity, and low toxicity [8,9]. One of the most appealing features of MSNs that make them highly attractive for delivery is the possibility of functionalizing the external surface of the material with sophisticated molecular, macromolecular or supramolecular ensembles to develop gated MSNs, which are able to demonstrate release in response to specific external stimuli [10]. In this particular field, a number of different gated-MSNs responding to light [11–14], pH [15–17], temperature [18–21], and certain bio-molecules [22–26] as stimuli have been described.

However, most MSN systems have their limitations, most importantly the limiting pore size of 2–3 nm. This small size restricts the cargo selection and MSN use in some pharmaceutical and biomedical applications. In particular, with this pore size, the vast majority of work done with release studies of MSNs utilizes dyes or smaller cytotoxic derivatives. Vitamins [27], or natural products such as garlic extract [28] have also been used as cargos. While another type of MSNs template, SBA-15, does have pore sizes sufficiently large for cargo such as cytochrome-C [29] or bovine serum albumin [30], the nanoparticle diameter itself is typically on the micrometer scale, thus drastically hindering its application toward certain in vivo uses. In this context, the strategy of expanding pores in MSNs is an appealing alternative method that shows potential in improving MSNs for larger cargo delivery. Two important and rapidly developing fields that take advantage of this are

peptide and gene therapy. Contrasting conventional drug delivery, which loads small molecules into MSNs, peptide and gene therapy use much larger species, such as proteins [31] or DNA [32]. However, despite these examples, the design of capped MSNs able to release large molecules is a field, which has not been fully explored.

An appealing physical stimulus that has been the focus of many applications in the field of controlled release is temperature. This stimulus was one of the first used in the design of hybrid organic–inorganic gated materials and a number of systems capped with thermo-responsive polymers [33] have been reported where fine cargo delivery control with paraffins [34] DNA and with [35], etc. was achieved using changes of temperature in the medium.

In addition to the thermoresponsive gating behavior, core-shell structured nanoparticles have recently been subject to extensive research for the combined functionalities of both the cores and outer layer, which enable them to be used in multiple applications. Some examples are nanoparticles consisting of a magnetic iron oxide core and silica shell [36]. These core-shell systems have shown great potential in particle separation, enzyme immobilization, and bio-applications [37]. For instance biocompatible superparamagnetic Fe_3O_4 has been widely used for in vivo biomedical applications including magnetic resonance imaging (MRI) contrast enhancement [38], hyperthermia [39], etc.

Based on these previous concepts, our aim presented here is to study the properties of core-shell mesoporous silica nanoparticles (CS–MSNs) with expanded pores and capped with the thermo-responsive polymer, PNIPAM, for protein release applications. PNIPAM undergoes a sharp conformational change at ca. 32 °C, at which, above this temperature, the polymer collapses from an extended brush. Previous studies have described the anchoring of this polymer on mesoporous supports [40–42]. The authors found that at low temperature the polymer was hydrated and extended closing the pores and inhibiting cargo delivery, whereas, at higher temperatures (above 32 °C), the polymer was in its hydrophobic and collapsed form allowing cargo release. The biocompatibility of PNIPAM has been debated in literature and while it does not biodegrade as other polymers such as polyethylene glycol or poly-lactic acid, it has been tested in several instances found in literature and shows little to no impact when used in low concentrations [41,42]. By this rationale, the in vivo performance of such PNIPAM-based nanoparticle delivery systems has been shown with various cell cultures, but intensive clinical studies are lacking. The inclusion of a magnetic core is solely a proof-of-concept that core-shell MSN based platforms can be used in conjunction with pore expansion and protein loading. It is our aim to demonstrate the potential use of the CS–MSNs to load lysozyme. Lysozyme is an antibacterial enzyme with an approximate diameter of ca. 3.9 nm which plays a crucial role in targeting Gram positive bacteria as a first line of defense in the human body [43,44]. Due to this, lysozyme is found abundantly in the nasal and ocular membranes and its deficiency often results in conjunctivitis or other increased incidences in illness [45]. The applicability of the temperature controlled delivery of lysozyme from CS–MSNs is tested by observing its antibacterial properties on Gram positive *Bacillus cereus* and *Micrococcus luteus* bacteria.

2. Materials and methods

2.1. Materials

Ferric chloride hexahydrate ($FeCl_3\,6H_2O$), ferrous chloride tetrahydrate ($FeCl_2\,4H_2O$), cetyltrimethylammonium bromide (CTAB), tetramethyl orthosilicate (TMOS), trimethylbenzene (TMB), (3-aminopropyl) triethoxysilane (APTES), α-bromoisobutyryl bromide (BIBB), *N*-isopropylacrylamide (NIPAM), copper (I) bromide (CuBr), *N,N,N′,N″,N″*-pentamethyldiethylenetrimine (PMDETA), and lysozyme from chicken egg white were purchased from Sigma–Aldrich and used as received. Ammonium hydroxide (NH_4OH), hydrochloric acid (HCl), sodium hydroxide (NaOH, pellets), ethanol, methanol, triethylamine (TEA), 2-propanol, and anhydrous toluene were purchased from Scharlab and used as received, unless otherwise noted. The Biotechnology Department of Polytechnic University of Valencia provided Colonies of *B. cereus* and *M. luteus*.

2.2. Synthesis of the Fe_3O_4/SiO_2 nanoparticles

The synthesis of the core shell mesoporous nanoparticles (CS–MSNs) follows a straightforward, stepwise reaction mechanism. The synthesis of the Fe_3O_4 cores was done by a co-precipitation method, using $FeCl_2$ and $FeCl_3$ precursor [36]. The MSN shells were produced by the sol–gel method using CTAB as the templating surfactant and TMOS as the silica precursor [32]. Pore expansion was done as follows. The dried CS–MSNs were dispersed in 10 mL of ethanol, ultrasonicated, and a 1:1 mixture of TMB/H_2O (20 mL total) was added and then autoclaved at 140 °C for 3 days. Afterwards, the nanoparticles were removed by centrifugation, copiously rinsed with ethanol and distilled water and dried at 60 °C to obtain CS–MSNs–EP.

2.3. Surface functionalization of amine and bromine groups

250 mg of CS–MSNs–EP were mixed with 10 mL of anhydrous toluene and 0.5 mL of APTES at 80 °C for 24 h. The nanoparticles were sonicated, centrifuged, and rinsed with ethanol and water, and then vacuum dried. The surfactant template was then removed through refluxing with acetone at 60 °C for 48 h, using fresh acetone after 24 h. From this, 150 mg were then mixed with 50 μL of TEA in 5 mL of anhydrous toluene. The mixture was cooled to 0 °C using an ice bath and 200 μL of BIBB in 2 mL of dry toluene was injected drop wise under Argon atmosphere. The reaction was carried out at 0 °C for 1 h and then allowed to increase to room temperature and continue for 24 h. The CS–MSNs–EP–BIBB were then filtered, rinsed with ethanol and water, and vacuum dried (see Scheme 1).

2.4. Atom transfer radical polymerization (ATRP) of PNIPAM

ATRP was used to graft PNIPAM onto CS–MSNs–EP–BIBB. A ratio of 25 mg of CS–MSNs–EP–BIBB to 0.25 g of NIPAM, 25 mg of CuBr, and 10 mL of 2-propanol/water (1:1) was used. Nitrogen gas was bubbled through the solution for 30 min and the entire system was purged with vacuum and flushed with Argon gas. Afterwards, 60 μL of PMDETA was injected into the system and polymerization run for 3 h. The resulting CS–MSNs–EP–PNIPAM nanoparticles were centrifuged and rinsed copiously with water (see Scheme 1).

2.5. Dye and lysoyzme loading/release

Loading with *tris*(bipyridine) ruthenium(II) chloride ($Ru(bipy)_3^{2+}$) dye was done prior to lysozyme to probe the efficacy of the PNIPAM gating. Briefly, two vials each containing 6 mg of $Ru(bipy)_3^{2+}$ and 10 mg of CS–MSNs–EP–PNIPAM were mixed in 1 mL of deionized water at 37 °C for 48 h. Afterwards, the nanoparticles were filtered and ice cold water was rinsed through the particles. The $Ru(bipy)_3^{2+}$ loaded nanoparticle (CS–MSNs–EP–PNIPAM-$Ru(bipy)_3^{2+}$) was dried in vacuum overnight at 25 °C. Release measurements were performed using two vials in their respective water baths, one designated for 25 °C and the other for 37 °C. At each designated time for the two vials, 200 μL was removed from each vial. The supernatant was collected from centrifugation at 10,000 rpm for 2 min and

then its fluorescence measured with a fluorospectrometer. The lysozyme loading and release was done in phosphate buffer saline (PBS 1X) prepared with the following quantities: 2 g NaCl, 50.9 mg KCl, 285 mg Na_2HPO_4, and 63.6 mg KH_2PO_4. Briefly, a solution of 50 mg lysozyme per 50 mg of CS–MSNs–EP–PNIPAM in 5 mL PBS 1X was prepared and gently stirred for 48 h at 37 °C. The rinsing and drying procedure of the final CS–MSNs–EP–PNIPAM–Lys were identical to the $Ru(bipy)_3^{2+}$ loaded system. The release was done similarly using water baths at 25 and 37 °C. Aliquots of 500 μL were removed at each time interval, centrifuged, and measured with UV/vis spectroscopy.

The amount of lysozyme loaded in the CS–MSNs–EP–PNIPAM–Lys was determined via absorption measurements of the lysozyme absorption band at 280 nm of the loading solution of lysozyme alone and after incubation with the CS–MSNs–EP–PNIPAM nanoparticles at 37 °C after a 48 h period:

$$[Lys] = [Lys_0] \left(\frac{loading\ \ abs - postloading\ \ abs}{loading\ \ abs} \right)$$

where [Lys] denotes the concentration of lysozyme that was uptaken into the CS–MSNs–EP–PNIPAM–Lys, $[Lys_0]$ is the concentration of lysozyme in the original loading solution, and *abs* is the absorbance measured from UV–vis spectrometry.

2.6. Bacteria culture conditions

For viability studies, Gram positive bacteria strains of *B. cereus* and *M. luteus* were used, kindly provided by the Biotechnology Department of UPV. All the bacterial experiments were performed in the Institute for Plant Molecular and Cellular Biology in UPV. Bacteria cells were grown and maintained in difco nutrient broth (DNB) medium supplemented with 2% of bacto-agar. For the assays, *B. cereus* and *M. luteus* cells were grown for 24 h at 28 °C and constant stirring with 5 mL of DNB medium. Then bacteria cells from 1 mL cultures were collected by centrifugation for 30 s at 13,000 rpm and resuspended in 1 mL of DNB medium. After that, a dilution of 10^6 cells/mL was prepared as the final working bacteria concentration. The same procedure was carried out for all viability assays.

2.7. Cytotoxicity assays

The in vivo assay consisted of a cytotoxicity analysis in 96-well plate format. Briefly, swabs of a colony of *B. cereus* and *M. luteus* were placed into difco nutrient broth medium and allowed to grow overnight at 28 °C. The following day, a mixed solution of bacteria and CS–MSNs–EP–PNIPAM–Lys was prepared, with a final bacterial concentration of 10^6–colonies/mL. The nanoparticle concentrations studied for CS–MSNs–EP–PNIPAM–Lys were 0.25 and 0.5 mg/mL in DNB medium. Also, a negative control was prepared in order to quantitate cell growth. The CS–MSNs–EP–PNIPAM–Lys bacterial solutions were then incubated with stirring at either 28 °C or 37 °C for 24 h. After the incubation time, bacterial growth was determined turbidimetrically through optical density measurements (OD_{620}) using a 96-well plate and an aliquot of 200 μL with a Thermo Scientific Multiskan FC multimode plate reader. CS–MSNs–EP–PNIPAM–Lys and growth medium solutions were included as baselines. Two replicates were prepared for each sample. Data represented are the mean ± S.E. of two independent experiments, giving *n* = 4 as a total sample size.

2.8. Characterization of materials

XRD was performed using Bruker AXS D8 Advance using Cu Kα radiation. TEM images were obtained from a JEOL2100F TEM at 100 kV accelerating voltage. A Malvern Zetasizer Nano ZS was used for the DLS measurements. Porosity characterization was done with a Micromeritics ASAP2020 using BJH method. Samples were degassed at 120 °C overnight prior to the analysis. UV–vis spectroscopy was done using a PerkinElmer Instruments Lambda 35 UV/vis spectrometer. Infrared spectroscopy (IR) was performed with a Bruker Platinum ATR. Optical turbidity measurements of the bacterial solutions were done using a Thermo Scientific Multiskan FC multimode plate reader.

3. Results and discussion

3.1. The PNIPAM-coated nanoparticles

As mentioned in the previous section, pore expansion to obtain CS–MSNs–EP was carried out by adding a suspension of the nanoparticles in ethanol to TMB/H_2O and the mixture then hydrothermally treated in an autoclave. The mechanism through which TMB expands the pores can be considered as a pseudomorphic transformation where the internal pore structure is changed [46]. The transformation implies a certain re-dissolution of the CS–MSNs favored through hydrothermal treatment. If so, each nanoparticle would behave like a nanoreactor in which incipient silica dissolution and self-assembling with in situ generated TMB-expanded micelles would occur with minimum and short-distance mass-transfer. By doing so, the pore surfactant micelle is expanded and the resulting porosity framework of the MSN is enlarged as well.

The expected performance of the final nanoparticles in terms of controlled release is shown in Scheme 2. The nanoparticles are expected to be capped at room temperature, whereas cargo delivery would be observed at physiological temperature.

3.2. Characterization of the nanoparticles

The prepared materials are characterized by standard techniques. Fig. 1 shows the powder X-ray diffraction (XRD) patterns of the CS–MSNs as-synthesized and the corresponding nanoparticles after pore expansion, i.e. CS–MSNs–EP. XRD at low angle of the CS–MSNs as-synthesized support shows the four typical low-angle reflections of a hexagonal-ordered mesoporous matrix indexed at (1 0 0), (1 1 0), (2 0 0) and (2 1 0) Bragg peaks (see Fig. 1a). Additionally, Fig. 1b displays the XRD of the CS–MSNs–EP after TMB hydrothermal treatment. In this case, all the low angle peaks completely disappear due to the complete reorganization of the internal mesostructure after pore expansion. As a result, no information regarding the possible porosity of these nanoparticles can be extracted from XRD data. A second feature in the XRD spectra of both the CS–MSNs and CS–MSNs–EP, shown in Fig. 1, is the presence of the characteristic peaks of Fe_3O_4 in the $28° < 2\theta < 68°$ range. The XRD of the Fe_3O_4 phase matches closely to similar systems previously reported [36]. The relative intensity of the Fe_3O_4 peaks slightly increase after the hydrothermal treatment in presence of TMB, taking into account as reference the intensity of the broad signal centered at ca. 25°, typical of non-ordered silica materials.

More information regarding the different morphology and texture of the CS–MSNs and CS–MSNs–EP can be obtained by transmission electron microscopy (TEM) studies. Fig. 2 shows the TEM images of the core-shell nanoparticles prior and after pore expansion. In the former, a porous appearance similar to that of a typical MCM-41 mesoporous phase is observed, whereas after exposure to TMB, the mesostructure is drastically modified. The original ordered pores evolve into larger and disordered pores. Moreover, TEM images (before and after the hydrothermal treatment) show dark spots associated to the Fe_3O_4 cores. The porosity of the meso-
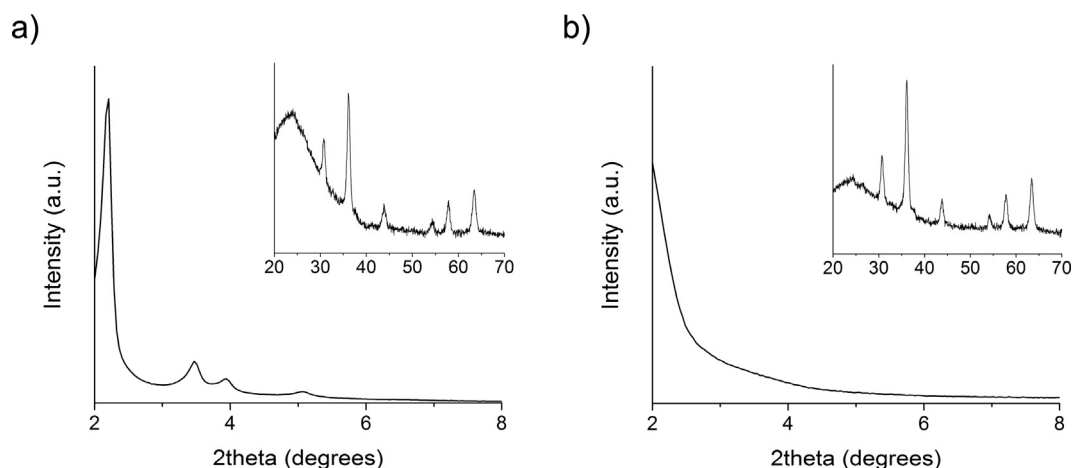
Fig. 1. Low angle XRD of (a) the as-synthesized CS–MSNs and (b) CS–MSNs–EP. Inset: high angle XRD showing the charatcteristic reflections of the Fe_3O_4 cores.

porous silica is difficult to observe in CS–MSNs–EP–PNIPAM due to the polymer coating around the nanoparticles.

N_2 Adsorption–desorption studies on CS–MSNs and CS–MSNs–EP were carried out in order to study the pore expansion in more detail. The N_2 adsorption–desorption isotherm of CS–MSNs is shown in Fig. 3. This curve shows two well-defined adsorption steps. The first, at an intermediate relative pressure ($0.2 < P/P_0 < 0.4$), is characteristic of type IV isotherms and can be related to capillary condensation of N_2 inside the intra-nanoparticle mesopores. The second and small step, at a high relative pressure ($P/P_0 > 0.9$), corresponds to the filling of the large pores among the primary nanoparticles and is associated to a small proportion of textural porosity. From the application of the BJH model on the adsorption branch of the isotherm, intraparticle mesopore diameter and pore volume are calculated to be 2.94 nm and 0.68 cm^3 g^{-1}, respectively (see Table 1). The absence of a hysteresis loop within this pressure range ($0.2 < P/P_0 < 0.4$) and the narrow BJH pore distribution suggest a cylindrical uniformity of the intraparticle mesopores. Additionally, using the BET model, a total specific area of 907.2 m^2 g^{-1} is calculated.

For CS–MSNs–EP, a smaller specific surface area (581.5 m^2 g^{-1}) but a larger N_2 adsorbed volume (0.86 cm^3 g^{-1}) is observed when compared with the CS–MSNs. Table 1 shows these values together with pore diameters and volume observed for the textural porosity for CS–MSNs–EP. N_2 adsorption–desorption studies allows the study of the pore expansion of CS–MSNs–EP when compared with CS–MSNs. Fig. 3b show the N_2 adsorption curve and the pore size distribution (in the inset) of the nanoparticles with expanded pores (CS–MSNs–EP). The two N_2 adsorption steps are preserved after the hydrothermal treatment. The shift of the first adsorption step towards higher relative pressure values ($0.4 < P/P_0 < 0.8$) is the confirmation of the pore expansion achieved. This step maintains a type-IV isotherm but with a marked H1 hysteresis loop. The pore size distribution curve shows a maximum centered at 6.07 nm and a broad shoulder extending to 9 nm. The larger mesopores and the wider pore size distribution observed when compared to the
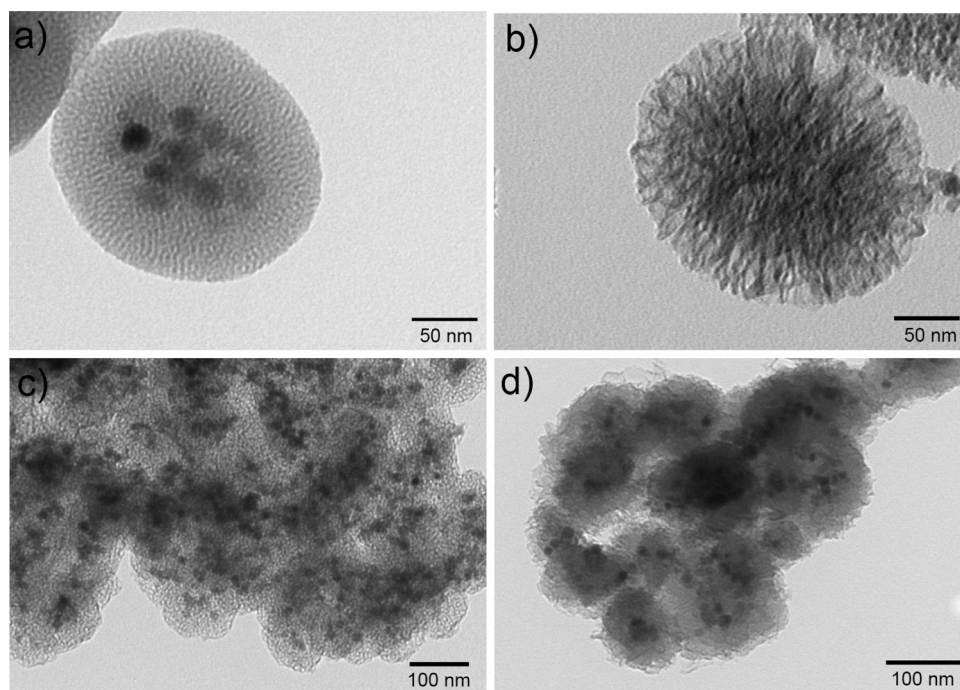

Fig. 2. TEM images of a single (a) CS–MSN, (b) CS–MSN–EP, and multiple (c) CS–MSNs–EP, and (d) CS–MSNs–EP–PNIPAM.
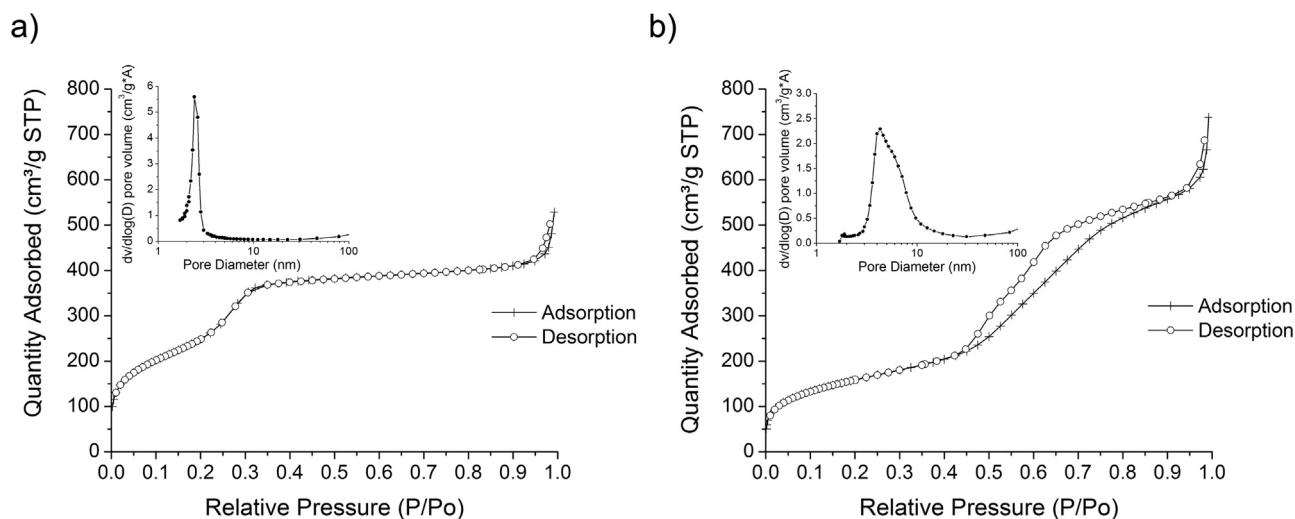
a)

b)

Fig. 3. Nitrogen adsorption–desorption isotherms for (a) CS–MSNs and (b) CS–MSNs–EP materials. The inset in (a) and (b) shows the pore size distribution of the CS–MSNs and CS–MSNs–EP materials, respectively.

Table 1
BET specific surface values, pore volumes and pore sizes calculated from the N_2 adsorption–desorption isotherms for CS–MSNs and CS–MSNs–EP.

	Specific surface (m^2/g)	Pore diameter (nm)	Specific volume (cm^3/g)	Pore diameter (nm)	Specific volume (cm^3/g)
		Mesopore		Textural pore	
CS–MSNs	907.2 ± 0.6	2.94(5)	0.68	39.3(8)	0.14
CS–MSNs–EP	581.5 ± 0.7	6.07(5)	0.86	54.5(9)	0.19

CS–MSNs derivatives are consistent with the information extracted from TEM images and XRD data.

Kim et al. [32] reported pore sizes up to 23 nm in diameter with a similar TMB treatment on mesoporous materials, but as seen here, the extent of pore expansion we obtain is 3–4 times less. While not investigated in depth, the core-shell structure seems to reduce the degree of pore expansion as for instance TMB as a pore-swelling agent with Fe_3O_4/SiO_2 core-shell nanoparticles was also used by Zhang et al. [47] and pores of only 3.77 nm size were reached. The difference here can be attributed to their selection of TMB addition directly to the vessel during MSN synthesis as opposed to the separate hydrothermal treatment done here. Nevertheless it is important to note that in the nanoparticles, most pore diameter values are greater than the 3.9 nm, which is the approximate diameter of lysozyme, indicating that pore-expanded CS–MSN is suitable for encapsulation of this enzyme.

Further studies using Fourier transform infrared spectroscopy (IR) were carried out in order to assess the functinalization process of the expanded-pore CS--MSNs–EP support with the PNIPAM polymer. Fig. 4(a) shows the IR spectra of the CS–MSNs–EP after subsequent additions of APTES, BIBB, and NIPAM (see Scheme 1). Amine bending, carboxyl, and amine stretch peaks can be observed at 1479, 1649, and 3300 cm^{-1}, respectively.

Moreover, the approximate hydrated diameter of the nanoparticles was studied by dynamic light scattering (DLS) measurements and the results are shown in Fig. 4(b). The CS–MSN–EP has an mean radius of ca. 110 nm, whereas the coresponding nanoparticles functionalized with PNIPAM (i.e. CS–MSNs–EP–PNIPAM) have a mean radius of 198 nm. The differences in the nanoparticle radius are ascribed to the surface functionalization with the PNIPAM polymer and the results indicate that the hydrated thickness of the polymer layer is ca. 88 nm. To demonstrate the thermoresponsive behavior of the PNIPAM polymer, dynamic light scattering (DLS) studies were also carried out for CS–MSNs–EP–PNIPAM at 40 °C. Fig. 4b shows that the change in thickness was about 27 nm, from a radius

of 198 nm to 171 nm, when the temperature is changed from 20 °C (the ambient room temperature) to 40 °C. This indicates that the collapsed PNIPAM polymer is about 61 nm in thickness. Additionally, the DLS studies show that the nanoparticles are dispersed and that no significant aggregates are observed.

3.3. Dye loading and release

For comparison purposes loading and delivery is also carried out with a relatively small dye such as $Ru(bipy)_3^{2+}$. As a part of the nanoparticle's design, the PNIPAM polymer is expected to inhibit cargo delivery, yet it is possible to trigger cargo release by changes in temperature. In order to test this possibility, delivery studies are performed at two different temperatures on the gated nanoparticles. In a first step delivery studies using CS–MSNs–EP–PNIPAM–$Ru(bipy)_3^{2+}$ loaded with the relatively small dye $Ru(bipy)_3^{2+}$ are performed. In a typical experiment CS–MSNs–EP–PNIPAM–$Ru(bipy)_3^{2+}$ are suspended in PBS1X and separated in 2 aliquots that were maintained at two different temperatures (i.e. 25 and 37 °C) and at certain times, fractions were taken and centrifuged to eliminate the nanoparticles. Cargo delivery to the solution is then determined by measuring the emission of the $Ru(bipy)_3^{2+}$ dye at 610 nm ($\lambda_{ex} = 460$ nm). Fig. 5(a) shows the delivery profile of the dye from CS–MSNs–EP–PNIPAM–$Ru(bipy)_3^{2+}$ at two temperatures. As it can be seen at 25 °C some $Ru(bipy)_3^{2+}$ delivery is observed, whereas at 37 °C the pores are opened as the PNIPAM polymer is in collapsed form, allowing a significantly larger cargo release.

From the release of $Ru(bipy)_3^{2+}$ for both room and physiological temperatures, it is concluded that the PNIPAM gates play a role in modulating the release, even for relatively small species such as the $Ru(bipy)_3^{2+}$ dye. Although the CS–MSNs–PNIPAM–$Ru(bipy)_3^{2+}$ at 37 °C shows favorable release, at 25 °C some dye release is also noticeable. This is likely be due to $Ru(bipy)_3^{2+}$ diffusing through the PNIPAM brushes from the mesoporous silica.
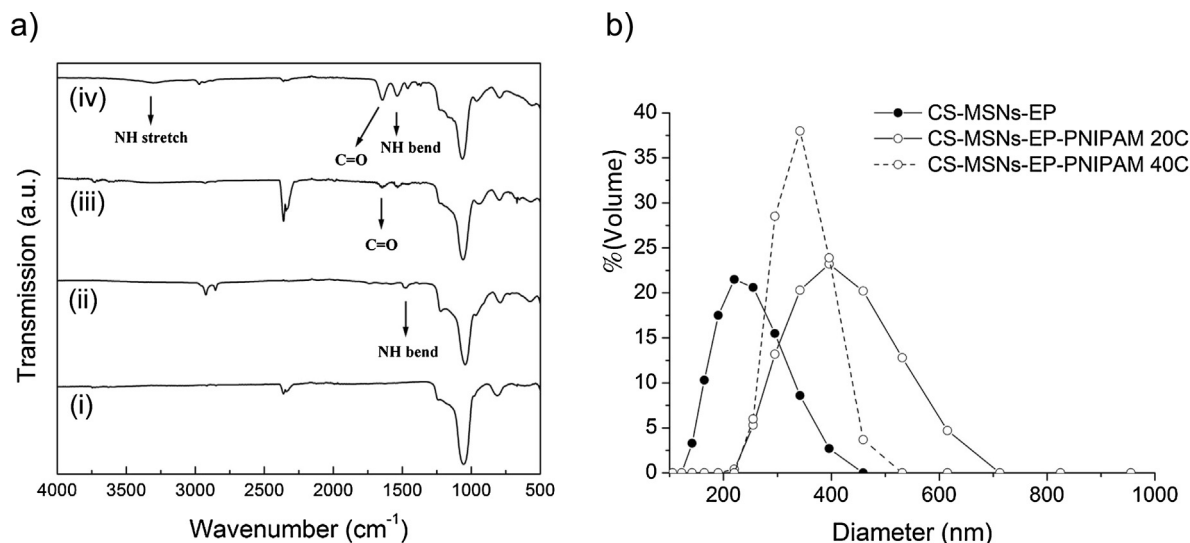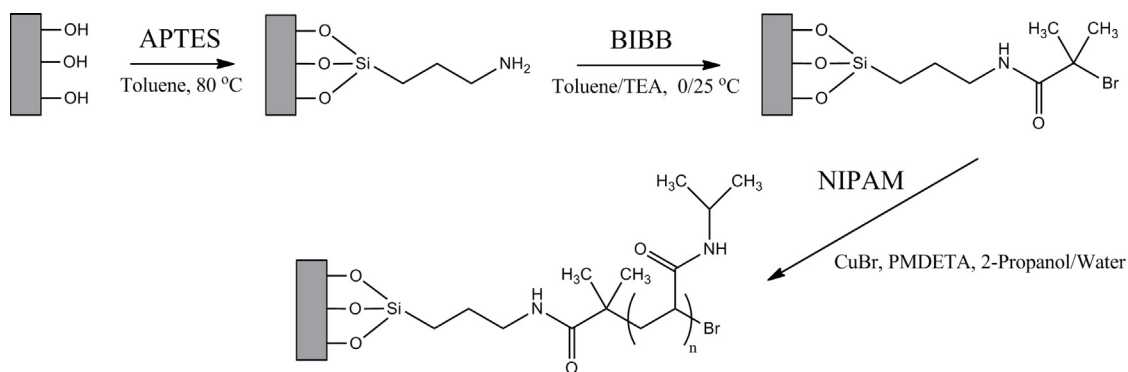
Fig. 4. (a) IR spectra of (i) expanded-pore the CS–MSNs–EP support, (ii) after APTES, (iii) after BIBB, (iv) and after PNIPAM functionalization. The occasional impurity peaks found near 2400 cm^{-1} are due to entrapped carbon dioxide content; (b) Size distribution from DLS measurement of CS–MSNs–EP and CS–MSNs–EP–PNIPAM at 20 °C and 40 °C. The hydrodynamic size change of the nanoparticles can be seen when the temperature was adjusted from 20 to 40 °C.
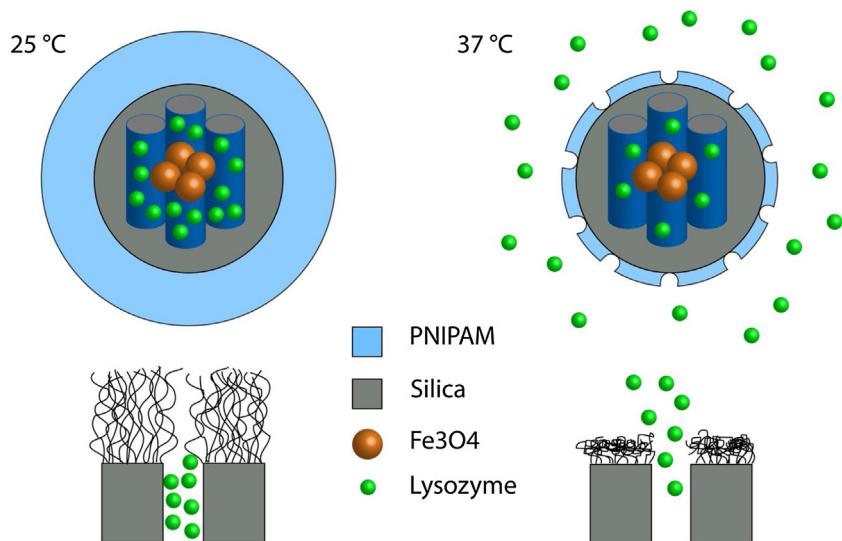

Scheme 1. Reaction mechanism showing the sequential steps toward ATRP grafting of PNIPAM on the CS–MSNs.

3.4. Lysozyme loading and release

Delivery studies using the CS–MSNs–EP–PNIPAM–Lys loaded with the enzyme lysozyme were performed in addition to dye. The amount of lysozyme loaded in the CS–MSNs–EP–PNIPAM–Lys is determined via absorption measurements of the lysozyme absorption band at 280 nm of the loading solution of lysozyme alone and after incubation with the CS–MSNs–EP–PNIPAM nanoparticles at

Scheme 2. Schematic drawing of the lysozyme release due to temperature in the CS–MSNs–PNIPAM.
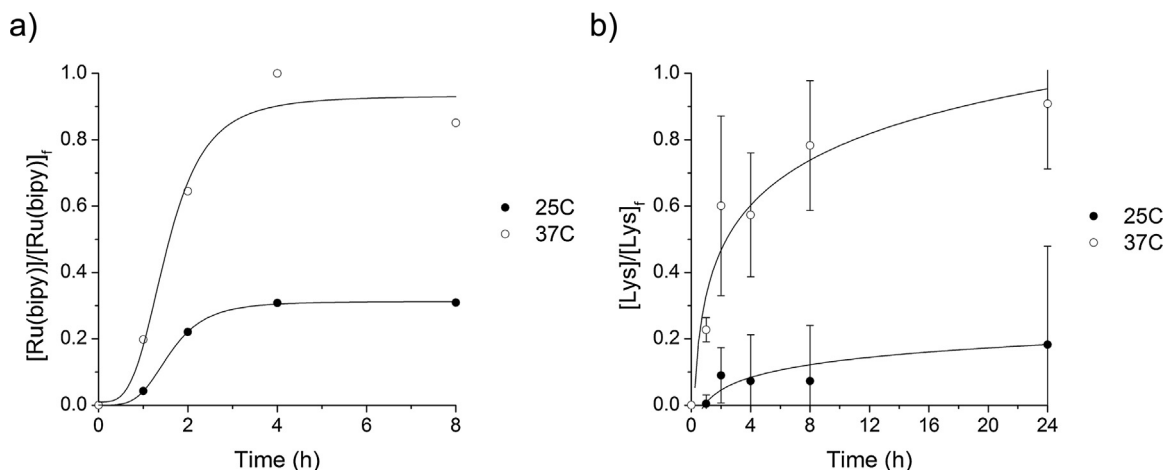
Fig. 5. (a) Release of Ru(bipy)$_3$$^{2+}$ dye from CS–MSNs–EP–PNIPAM–Ru(bipy)$_3$$^{2+}$ as measured by fluorospectroscopy for the $n = 1$ experiments performed; (b) release of lysozyme from the CS–MSNs–PNIPAM–Lys at both 25 and 37 °C over 24 h for the $n = 3$ experiments performed.

37 °C after a 48 h period. Using this procedure the amount of loaded lysozyme is determined to be ca. 160 mg/g which is reasonable in comparison to other lysozyme-SBA-15 loading results [48]. Delivery experiments for CS–MSNs–EP–PNIPAM–Lys at 25 and 37 °C are carried out using a similar protocol to that described above for the CS–MSNs–EP–PNIPAM–Ru(bipy)$_3$$^{2+}$ and the results are shown in Fig. 5(b). In this case lysozyme delivery to the solution is then determined by measuring the absorption at 280 nm.

Similar to that found in the delivery of Ru(bipy)$_3$$^{2+}$ dye from CS–MSNs–EP–PNIPAM–Ru(bipy)$_3$$^{2+}$ at 25 °C, an immediate brief increase in the absorbance is detected within 2 h which may be result of residual lysozyme desorbing from the PNIPAM brushes. However the release is marginal after the 2 h period. In contrast, at 37 °C, release of lysozyme continues at a greater extent. From previous studies using SBA-15 templates, near complete lysozyme release was seen in drastically less than 1 h [49] to some cases where it extended to nearly 300 h [48]. In our case lysozyme delivery takes aproximately 24 h. When the delivery of Ru(bipy)$_3$$^{2+}$ and lysozyme are compared, it is clear that a much faster release is obtained for Ru(bipy)$_3$$^{2+}$ when compared with lysozyme (see Fig. 5a and b). In particular, whereas maximum Ru(bipy)$_3$$^{2+}$ delivery is observed after ca. 4 h, maximum delivery of lysozyme is only observed after ca. 24 h. This difference is clearly due to the smaller dimensions of the Ru(bipy)$_3$$^{2+}$ dye when compared with

the enzyme. Moreover the results demonstrate that it is possible to design CS–MSNs–EP nanoparticles with large enough pores to load macromolecules such as lysozyme and that it is possible to control delivery of cargo as a function of temperature using the PNIPAM polymer.

3.5. Cytotoxicity assays

Overuse of antibacterial agents and as a result, bacterial resistance to common antibiotics, is a serious concern for modern medicine [50]. Because of this the design of non-traditional antibiotic agents, based on nano-formulations, has become of interest [51]. In this context the temperature-controlled delivery of lysozyme from CS–MSNs–EP–PNIPAM–Lys was tested by taking advantage of the antibacterial properties of lysozyme. In particular the ability of lysozyme to break down Gram positive cell walls in bacteria serves as an excellent method to characterize the effectiveness of the nanoparticles as a potential systems able to release this enzyme in a temperature-controlled manner. For this study colonies of *B. cereus* and *M. luteus* are used. In a typical experiment the bacteria are allowed to grow overnight at 28 °C and the following day a mixed solution of bacteria and CS–MSNs–EP–PNIPAM–Lys is prepared, with a final bacterial concentration of 10^6 colonies/mL. The CS–MSNs–EP–PNIPAM–Lys
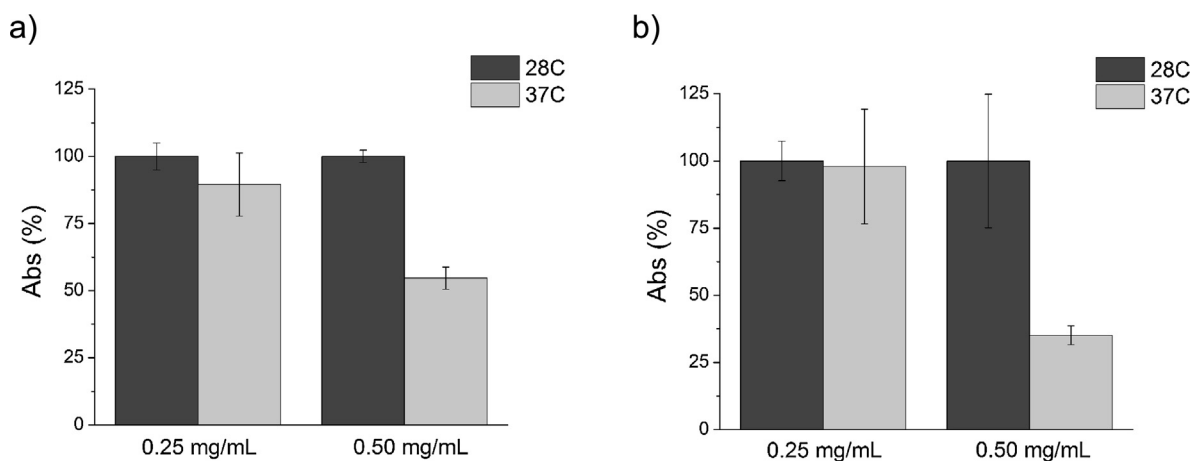

Fig. 6. (a) Effect of the lysozyme loaded CS–MSNs–EP–PNIPAM–Lys on solutions of *Bacillus cereus* and (b) *Micrococcus luteus*. Optical density measurements are done at 620 nm after 5 s of shaking. Concentrations of 0.25 and 0.50 mg/mL of nanoparticles are used. Data represented are the mean ± S.E. of two independent experiments each one done in duplicate.

concentrations tested are 0.25 and 0.5 mg/mL in DNB medium. The solutions containing CS–MSNs–EP–PNIPAM–Lys and the corresponding bacteria are incubated with stirring at either 28 °C or 37 °C for 24 h and then bacterial growth is determined turbidimetrically (OD_{620}). The time period of 24 h is selected both because to minimize longer duration effects such as differing phases in the bacterial growth curve (natural slowing) and a decaying release observed from Fig. 5b after 24 h. In these experiments blank measurements of only bacteria, only CS–MSNs–EP–PNIPAM–Lys, and only growth medium solutions are used as baselines in order to remove effects that the nanoparticles can have on bacterial growth.

From the results in Fig. 6, it is observed that there is not a substantial difference in bacterial growth between the two temperaures in the presence of CS–MSNs–EP–PNIPAM–Lys at a concentration of 0.25 mg/mL, while in contrast a clear temperature dependent bioability is observed at a concentration of nanoparticles of 0.50 mg/mL. In this case bacteria growth show a near 60% reduction for *B. cereus* and 45% for *M. luteus*, of the original colony count, when the temperature is set to 37 °C as opposed to the results at 25 °C. Given the lack of extensive lysozyme release studies that also have been quantified through bacteria colony counting, this 45–60% reduction is difficult to interpret in comparison to other systems. The starting colony count of 10^6 colonies/mL is not unusual, ranging within 1–2 orders of magnitude of other antibacterial studies [52–54] but the delivery species here is lysozyme, not a smaller, antibiotic compound such as vancomycin, a typical benchmark species used frequently. The loading extent and antimicrobial efficiency differ greatly between enzymatic and antibiotic approaches. The reduction in colony count is reasonable in accordance with other studies involving antibiotic release from mesoporous silica nanoparticles, where a 70% reduction in *E. coli* colony count was observed after 24 h using allyl isothiocyanate as the antimicrobial loading species [53]. The experiments presented here indicate that lysozyme-loaded nanoparticles are not toxic at room temperature but are toxic at physiological temperature due to a selective temperature-controlled release of lysozyme and the antibacterial properties of this enzyme.

4. Conclusion

New core-shell nanoparticles containing of Fe_3O_4 cores and an expanded pore mesoporous silica shell, loaded with $Ru(bipy)_3^{2+}$ dye or lysozyme and capped with the thermoresponsive PNIPAM polymer have been prepared and characterized. Pore expansion was achieved with TMB and the PNIPAM coating was done using ATRP. N_2 adsorption–desorption studies on the expanded pore material showed an average pore diameter of 6.07 nm. Both final nanoparticles (i.e. CS–MSNs–EP–PNIPAM–$Ru(bipy)_3^{2+}$ and CS–MSNs–EP–PNIPAM–Lys) displayed some cargo delivery at room temperature yet a significant larger release was observed at 37 °C when the polymer was in its hydrophobic and collapsed form. A faster release was observed for CS–MSNs–EP–PNIPAM–$Ru(bipy)_3^{2+}$ when compared with CS–MSNs–EP–PNIPAM–Lys due to the smaller dimensions of the $Ru(bipy)_3^{2+}$ dye when compared with the enzyme. Moreover the responsive behavior of CS–MSNs–EP–PNIPAM–Lys was studied at different temperatures for the selective delivery of lysozyme in the presence of Gram-positive bacteria *B. cereus* and *M. luteus*. The results demonstrated that the nanoparticles were not toxic for bacteria at a concentration of 0.50 mg/mL at 25 °C, whereas delivery of lysozyme at 37 °C resulted in a remarkable reduction of bacteria growth.

References

[1] Gai S. Yang P, J. Lin, Functionalized mesoporous silica materials for controlled drug delivery, Chem. Soc. Rev. 41 (2012) 3679–3698.

[2] I.I. Slowing, B.G. Trewyn, S. Giri, V.S.-Y. Lin, Mesoporous silica nanoparticles for drug delivery and biosensing applications, Acc. Chem. Res. 17 (2007) 1225–1236.

[3] E. Aznar, R. Martínez-Máñez, F. Sancenón, Controlled release using mesoporous materials containing gate-like scaffoldings, Exp. Opin. Drug Delivery 6 (2009) 643–655.

[4] M. Delcea, H. Möhwald, A.G. Skirtach, Stimuli-Responsive LbL capsules and nanoshells for drug delivery, Adv. Drug DeliveryRev. 63 (2011) 730–747.

[5] B.P. Tiwari, B.R. Rane, N.A. Gujarathi, S.P. Pawar, An overview: sustained release drug delivery technologies with polymeric systems, Pharm. Sci. Monit. 4 (2013) 3506–3521.

[6] P.R. Cullis, L.D. Mayer, M.B. Bally, T.D. Madden, M.J. Hope, Generating and loading of liposomal systems for drug-delivery applications, Adv. Drug Delivery Rev. 3 (1989) 267–282.

[7] A.M. Alaouie, S. Sofou, Liposomes with triggered content release for cancer therapy, J. Biomed. Nanotechnol. 4 (2008) 234–244.

[8] A.P. Wright, M.E. Davis, Design and preparation of organic-inorganic hybrid catalysts, Chem. Rev. 102 (2002) 3589–3614.

[9] G. Kickelbick, Hybrid inorganic-organic mesoporous materials, Angew. Chem. Int. Ed. 43 (2004) 3102–3104.

[10] C. Coll, A. Bernardos, R. Martínez-Máñez, F. Sancenón, Gated silica mesoporous supports for controlled release and signaling applications, Acc. Chem. Res. 46 (2013) 339–349.

[11] E. Aznar, M.D. Marcos, R. Martínez-Máñez, F. Sancenón, J. Soto, P. Amorós, C. Guillem, pH- and photo-switched release of guest molecules from mesoporous silica supports, J. Am. Chem. Soc. 131 (2009) 6833–6843.

[12] N.K. Mal, M. Fujiwara, Y. Tanaka, Photocontrolled reversible release of guest molecules from coumarin-modified mesoporous silica, Nature 421 (2003) 350–353.

[13] T.M. Guardado-Alvarez, L.D. Devi, M.M. Russell, B.J. Schwartz, J.I. Zink, Activation of snap-top capped mesoporous silica nanocontainers using two near-infrared photons, J. Am. Chem. Soc. 135 (2013) 14000–14003.

[14] C. Park, K. Lee, C. Kim, Photoresponsive cyclodextrin-covered nanocontainers and their sol–gel transition induced by molecular recognition, Angew. Chem. Int. Ed. 48 (2009) 1275–1278.

[15] Q. Yang, S. Wang, P. Fan, L. Wang, Y. Di, K. Lin, F.-S. Xiao, pH-Responsive carrier system based on carboxylic acid modified mesoporous silica and polyelectrolyte for drug delivery, Chem. Mater. 17 (2005) 5999–6003.

[16] S. Wu, X. Huang, X. Du, Glucose- and pH-responsive controlled release of cargo from protein-gated carbohydrate-functionalized mesoporous silica nanocontainers, Angew. Chem. Int. Ed. 52 (2013) 5580–5584.

[17] H. Meng, M. Xue, T. Xia, Y.-L. Zhao, F. Tamanoi, J.F. Stoddart, J.I. Zink, A.E. Nel, Autonomous in vitro anticancer drug release from mesoporous silica nanoparticles by pH-sensitive nanovalves, J. Am. Chem. Soc. 132 (2010) 12690–12697.

[18] Z. Yu, N. Li, P. Zheng, W. Pan, B. Tang, Temperature-responsive DNA-gated nanocarriers for intracellular controlled release, Chem. Commun. 50 (2014) 3494–3497.

[19] A. Baeza, E. Guisasola, E. Ruiz-Hernández, M. Vallet-Regí, Magnetically triggered multidrug release by hybrid mesoporous silica nanoparticles, Chem. Mater. 24 (2012) 517–524.

[20] C. de la Torre, A. Agostini, L. Mondragón, M. Orzáez, F. Sancenón, R. Martínez-Máñez, M.D. Marcos, P. Amorós, E. Pérez-Payá, Temperature-controlled release by changes in the secondary structure of peptides anchored onto mesoporous silica supports, Chem. Commun. 50 (2014) 3184–3186.

[21] Y. Zhu, S. Kaskel, T. Ikoma, N. Hanagata, Magnetic SBA-15/poly(*N*-isopropylacrylamide) composite: preparation,

characterization and temperature-responsive drug release property, Microporous Mesoporous Mater. 123 (2009) 107–112.

[22] Y. Zhu, W. Meng, H. Gao, N. Hanagata, Hollow mesoporous silica/poly(L-lysine) particles for codelivery of drug and gene with enzyme-triggered release property, J. Phys. Chem. C 115 (2011) 13630–13636.

[23] Y. Zhao, B.G. Trewyn, I.I. Slowing, V.S.Y. Lin, Mesoporous Silica nanoparticle-based double drug delivery system for glucose-responsive controlled release of insulin and cyclic AMP, J. Am. Chem. Soc. 131 (2009) 8398–8400.

[24] E. Climent, R. Martínez-Máñez, F. Sancenón, M.D. Marcos, J.A. Soto Maquieira, P. Amorós, Controlled delivery using oligonucleotide-capped mesoporous silica nanoparticles, Angew. Chem. Int. Ed. 49 (2010) 7281–7283.

[25] E. Climent, R. Martínez-Máñez, A. Mqueira, F. Sancenón, M.D. Marcos, E.M. Brun, J. Soto, P. Amorós, Antibody-capped mesoporous nanoscopic materials: design of a probe for the selective chromo-fluorogenic detection of finasteride, ChemOpen 1 (2012) 251–259.

[26] E. Aznar, R. Villalonga, C. Giménez, F. Sancenón, M.D. Marcos, R. Martínez-Máñez, P. Díez, J.M. Pingarrón, P. Amorós, Glucose-triggered release using enzyme-gated mesoporous silica nanoparticles, Chem. Commun. 49 (2013) 6391–6393.

[27] A. Bernardos, E. Aznar, C. Coll, R. Martínez-Máñez, J.M. Barat, M.D. Marcos, F. Sancenón, A. Benito, J. Soto, Controlled release of vitamin B2 using mesoporous materials functionalized with amine-bearing gate-like scaffoldings, J. Control. Release 131 (2008) 181–189.

[28] C. Acosta, E. Pérez-Esteve, C.A. Fuenmayor, S. Benedetti, M.S. Cosio, J. Soto, F. Sancenón, S. Mannino, J. Barat, M.D. Marcos, R. Martínez-Máñez, Polymer composites containing gated mesoporous materials for on-command controlled release, ACS Appl. Mater. Inter. 6 (2014) 6453–6460.

[29] I. Slowing, G. Trewyn, V.S.Y. Lin, Mesoporous silica nanoparticles for intracellular delivery of membrane-impermeable proteins, J. Am. Chem. Soc. 129 (2007) 8845–8849.

[30] S.W. Song, K. Hidajat, S. Kawi, Functionalized SBA-15 materials as carriers for controlled drug delivery: influence of surface properties on matrix-drug interactions, Langmuir 21 (2005) 9568–9575.

[31] M.M. Wan, J.Y. Yang, Y. Qiu, Y. Zhou, C.X. Guan, Q. Hou, W.G. Lin, J.H. Zhu, Sustained release of heparin on enlarged-pore and functionalized MCM-41, ACS Appl. Mater. Inter. 4 (2012) 4113–4122.

[32] M.-H. Kim, H.-K. Na, Y.-K. Kim, S.-R. Ryoo, S. Cho, E. Lee, H. Jeon, R. Ryoo, D.-H. Min, Facile synthesis of monodispersed mesoporous silica nanoparticles with ultralarge pores and their application in gene delivery, ACS Nano 5 (2011) 3568–3576.

[33] Y.-Z. You, K.K.S.L. Kalebaila Brock, D. Oupický, Temperature-controlled uptake and release in PNIPAM-modified porous silica nanoparticles, Chem. Mater. 20 (2008) 3354–3359.

[34] E. Aznar, L. Mondragón, J.V. Ros-Lis, F. Sancenón, M.D. Marcos, R. Martínez-Máñez, J. Soto, E. Pérez-Payá, P. Amorós, Finely tuned temperature-controlled cargo release using paraffin-capped mesoporous silica nanoparticles, Angew. Chem. Int. Ed. 50 (2011) 11172–11175.

[35] E. Ruiz-Hernández, A. Baeza, M. Vallet-Regí, Smart drug delivery through DNA/magnetic nanoparticle gates, Acs. Nano 5 (2011) 1259–1266.

[36] E. Bringas, Ö. Köysüren, D.V. Quach, M. Mahmoudi, E. Aznar, J.D. Roehling, M.D. Marcos, R. Martínez-Máñez, P. Stroeve, Triggered release in lipid bilayer-capped mesoporous silica nanoparticles containing SPION using an alternating magnetic field, Chem. Commun. 48 (2012) 5647–5649.

[37] J. Yang, D. Shen, L. Zhou, W. Li, X. Li, C. Yao, R. Wang, A.M. El-Toni, F. Zhang, D. Zhao, Spatially Confined fabrication of Core–Shell Gold nanocages@mesoporous silica for near-infrared controlled photothermal drug release, Chem. Mater. 25 (2013) 3030–3037.

[38] N. Nitin, L. LaConte, O. Zurkiya, X. Hu, G. Bao, Functionalization and peptide-based delivery of magnetic nanoparticles as an intracellular MRI contrast agent, J. Biol. Inorg. Chem. 9 (2004), 706–712.

[39] K. Hayashi, K. Ono, H. Suzuki, M. Sawada, M. Moriya, W. Sakamoto, T. Yogo, High-Frequency, magnetic-field-responsive drug release from magnetic nanoparticle/organic hybrid based on hyperthermic effect, ACS Appl. Mater. Inter. 2 (2010) 1903–1911.

[40] C. Liu, J. Guo, W. Yang, J. Hu, C. Wang, S. Fu, Magnetic mesoporous silica microspheres with thermo-sensitive polymer shell for controlled drug release, J. Mater. Chem. 19 (2009) 4764–4770.

[41] B. Chang, X. Sha, J. Guo, Y. Jiao, C. Wang, W. Yang, Thermo and pH dual responsive, polymer shell coated, magnetic mesoporous silica nanoparticles for controlled drug release, J. Mater. Chem. 21 (2011) 9239–9247.

[42] Yang Yang, et al., Preparation of polymer-coated mesoporous silica nanoparticles used for cellular imaging by a graft-from method, J. Mater. Chem. 18 (2008) 5731–5737.

[43] M. Arabski, I. Konieczna, E. Tusinska, S. Wasik, I. Relich, K. Zajac, Z. Kaminski, W. Kaca, The use of lysozyme modified with fluorescein for the detection of gram-positive bacteria, Microbiol. Res. (2014), http://dx.doi.org/10.1016/j.micres.2014.05.004.

[44] S. Kroll, C. Brandes, J. Wehling, L. Treccani, G. Grathwohl, K. Rezwan, Highly efficient enzyme -functionalized porous zirconia microtubes for bacteria filtration, Enviorn. Sci. Technol. 16 (2012) 8739–8747.

[45] K.-J. Lin, S.-L. Chen, Physicochemical properties of lysozyme and its role in disease, Lysozymes (2013) 179–191.

[46] A. Galarneau, J. Iapichella, K. Bonhomme, F. Di Renzo, P. Kooyman, O. Terasaki, F. Fajula, Controlling the morphology of mesostructured silicas by pseudomorphic transformation: a route towards applications, Adv. Funct. Mater. 16 (2006) 1657–1667.

[47] J. Zhang, X. Li, J.M. Rosenholm, H.-C. Gu, Synthesis and characterization of pore size-tunable magnetic mesoporous silica nanoparticles, J. Colloid Interface Sci. 361 (2011) 16–24.

[48] M.S. Bhattacharyya, P. Hiwale, M. Piras, L. Medda, D. Steri, M. Piludu, A. Salis, M. Monduzzi, Lysozyme adsorption and release from ordered mesoporous materials, J. Phys. Chem. C 114 (2010) 19928–19934.

[49] S. Huang, C. Li, P. Yang, C. Zhang, Z. Cheng, Y. Fan, J. Lin, Luminescent CaWO$_4$: Tb^{3+}-loaded mesoporous silica composites for the immobilization and release of lysozyme, Eur. J. Inorg. Chem. (2010) 2655–2662.

[50] A.M. Allahverdiyev, K.V. Kon, E.S. Abamor, M. Bagirova, M. Rafailovich, Coping with antibiotic resistance: combining nanoparticles with antibiotics and other antimicrobial agents, Exp. Rev. Anti-Infect. Ther. 9 (2011) 1035–1052.

[51] N. Mas, I. Galiana, L. Mondragón, E. Aznar, E. Climent, N. Cabedo, F. Sancenón, J.R. Murguía, R. Martínez-Máñez, M.D. Marcos, P. Amorós, Enhanced efficacy and broadening of antibacterial action of drugs via the use of capped mesoporous nanoparticles, Chem. Eur. J. 19 (2013) 11167–11171.

[52] I. Sondi, Branka Salopek-Sondi. Silver nanoparticles as antimicrobial agent: a case study on *E. coli* as a model for gram-negative bacteria, J. Colloid Interface Sci. 275 (2004) 177–182.

[53] Park, Sun-Young, Mary Barton, Phillip Pendleton, Mesoporous silica as a natural antimicrobial carrier, Colloids Surf. A 385 (2011) 256–261.

[54] Meng-Hua Xiong, et al., Lipase-sensitive polymeric triple-layered nanogel for on-demand drug delivery, J. Am. Chem. Soc. 134 (2012) 4355–4362.